Eigenvalue Spectrum of Marginally Outer Trapped Surface Stability Operator in the Weyl-Distorted Schwarzschild Black Holes

by

© **Okpala Chiamaka Mary**

A thesis submitted to the School of Graduate Studies in partial fulfillment of the requirements for the degree of Master of Science.

Department of Physics and Physical Oceanography

Memorial University

May 2025

St. John's, Newfoundland and Labrador, Canada

Abstract

Marginally outer trapped surfaces (MOTS) are closed spacelike surfaces from which outgoing light rays neither converge nor diverge. In recent years they have been found to be a key tool for understanding black hole geometries. In particular, the stability operator provides information on whether the marginally outer trapped surfaces (MOTS) bounds a trapped region. This study investigates the eigenvalue problem associated with the stability operator for MOTS in the context of Weyl-distorted Schwarzschild solutions. By solving the eigenvalue problem, we aim to understand whether these solutions can always be understood as black holes.

Keywords: Black holes, marginally outer trapped surfaces (MOTS), stability operator, Weyl-distorted Schwarzschild solutions.

Acknowledgements

I would like to acknowledge the territory on which Memorial University of Newfoundland and Labrador, St. John's campus, stands as the ancestral homelands of the Beothuk, and the island of Newfoundland as the ancestral homelands of the Mi'kmaq and Beothuk. I also recognize the Inuit of Nunatsiavut and NunatuKavut, and the Innu of Nitassinan, along with their ancestors, as the original people of Labrador. Their rich histories and cultures form the foundational fabric of this land.

To my supervisor, Prof. Ivan Booth: thank you for taking a gravitational leap of faith in me. Despite my background, your trust in me was unwavering. Your support, patience, and mentorship have been a constant force, shaping not just my academic trajectory but inspiring me to aim for greater heights.

To my family: my parents, Mr. and Mrs. Peter and Juliana Okpala, and my brothers Cyprian, George, Stephen, and Jude—your support has been constant in my life. From your prayers and encouragement, you've anchored me through life's uncertainties. I owe you more than words can express—dalu nu o!

To the Gravity Journal Club at MUN and my colleagues, Matin and Ayon: you might not realize it, but those meetings were a lifeline—thank you for your patience and for never running away when my barrage of questions came your way. Those discussions and insights have been invaluable.

A heartfelt thank you to all the professors in the Math and Physics department who have helped shape my academic journey: Graham Cox, Herman David Leigh, Hilding Neilson, and Juan Margalef. Your wisdom and guidance have been instrumental. Finally and most importantly, my deepest gratitude to Jesus Christ—for the strength to persevere and for the grace that has carried me this far.

As the Igbo tribe of Nigeria would say: "Dalu nu o!"

Statement of contribution

Part of section 2.2, *the Weyl-distorted Schwarzschild solution*, as well as the entirety of the spectral method analysis and its results in subsection 5.1.1, are based on the unpublished manuscript by I. Booth, G. Cox, and C.M. Okpala, titled:

"Blackhole Dissolution"

Department of Mathematics, Memorial University of Newfoundland.

Author Contributions

The contributions of the authors to this thesis are as follows:

Prof. Ivan Booth: My supervisor and co-primary investigator made significant contributions to the theoretical foundations of this work. Specifically, he developed the subsections on the Einstein field equations distortion potentials and the exact series solution for the distortion potentials, all in section 2.2 of chapter 2. Additionally, Prof. Booth conducted the numerical spectral method analysis for the operator and derived the corresponding results. His guidance throughout this process has been invaluable, and I am deeply grateful for his mentorship.

C.M. Okpala: As the author of this thesis, my specific contributions include:

1. Writing and structuring the thesis, with valuable editing assistance and feedback from Prof. Booth.

2. Conducting the finite difference method (FDM) analysis of the operator, providing an independent computational perspective to complement the spectral method analysis.

3. Performing a detailed comparison of the results, which demonstrated their consistency and agreement. This comparison was crucial for validating the findings.

Table of contents

List of figures

List of symbols

R	real numbers
Σ	3-dimensional spacelike hypersurface of M
S	2-dimensional closed, smooth hypersurface embedded in Σ
q_{ab}	Induced metric on Σ
Λ	Cosmological constant
K	Gaussian curvature on S within Σ
R	Scalar curvature for (M, g)
θ_n	Inward null expansion
θ_l	outward null expansion
L	Stability operator
ω_a	Connection of the normal bundle on S

Chapter 1

INTRODUCTION

1.1 The Enigma of Black Holes

Black holes are among the most mysterious and enigmatic objects in the cosmos. These regions of spacetime are defined by such immense gravity that not even light can escape their pull [27]. The concept of black holes arises from Einstein's theory of General Relativity. This theory suggests that when a mass becomes sufficiently compact, it warps spacetime to such an extent that a black hole forms [16]. Several key features define these cosmic phenomena. The first is the Event Horizon—the invisible boundary surrounding a black hole, beyond which escape becomes impossible because the required speed exceeds that of light [36]. For a static, spherically symmetric black hole in vacuum, this boundary is at the Schwarzschild radius:

$$r_s = \frac{2Gm}{c^2}. \tag{1.1}$$

Here, G is the gravitational constant, m is the mass of the black hole, and c is the speed of light [49]. Within the event horizon lies the singularity, a point where the

spacetime curvature becomes infinite, and our current understanding of physics fails to describe the conditions [40].

The story of gravity itself is one of the most remarkable journeys in the history of science. Isaac Newton's law of universal gravitation was the first successful theory to describe the attraction between masses [38]. Newton proposed that every particle in the universe attracts every other particle with a force inversely proportional to the square of the distance between them:

$$F = \frac{Gm_1m_2}{r^2}. \tag{1.2}$$

This equation, where F is the gravitational force between two masses m_1 and m_2 separated by a distance r, and G is the gravitational constant, became a cornerstone of classical mechanics that beautifully explained physical scenarios such as the motion of planets and moons but fell short in accounting for certain phenomena, like the bending of light or the peculiar orbit of Mercury [33]. These puzzles hinted at the need for a new understanding of gravity [60].

Enter Albert Einstein, who, in 1915, revolutionized our understanding of gravity with his general theory of relativity. Instead of viewing gravity as a force, Einstein described it as a curvature of spacetime caused by mass and energy [17]. Massive objects like the Sun bend the fabric of spacetime, and this curvature dictates the motion of objects, much like a marble rolling along a curved surface. This elegant theory not only explained the anomalies in Mercury's orbit but also predicted the bending of light by gravity, both of which were later confirmed by observations [15].

At the heart of Einstein's theory are the field equations:

$$R_{\mu\nu} - \frac{1}{2}Rg_{\mu\nu} + \Lambda g_{\mu\nu} = \frac{8\pi G}{c^4}T_{\mu\nu}. \tag{1.3}$$

These equations describe how matter and energy influence the curvature of spacetime, with $R_{\mu\nu}$ representing the Ricci curvature tensor, R the Ricci scalar, $g_{\mu\nu}$ the metric tensor, Λ the cosmological constant, and $T_{\mu\nu}$ the stress-energy tensor [17]. They outline a dynamic relationship between spacetime and the distribution of matter and energy, giving rise to various gravitational phenomena [31] such as the equivalence principle, which states that the effects of gravity are indistinguishable from those of acceleration within a local inertial frame. This principle led to the realization that free-falling particles follow geodesics through spacetime, analogous to Riemannian geodesics (see Figure 1.1), which represent paths of extremal length between fixed points in curved space.

1.2 Geodesics in General Relativity

In the familiar geometry of flat, Euclidean space, the shortest path between two points is a straight line. However, in the context of curved spacetime, as described by general relativity, the closest analog to a straight line is a geodesic. Geodesics represent the paths that objects follow when they are under the influence of gravity alone, without any additional forces. The geodesic equation mathematically describes this path as:

$$\frac{d^2x^\mu}{d\tau^2} + \Gamma^\mu_{\alpha\beta}\frac{dx^\alpha}{d\tau}\frac{dx^\beta}{d\tau} = 0, \tag{1.4}$$

where x^μ denotes the coordinates in spacetime, τ is the proper time experienced by the moving object, and $\Gamma^\mu_{\alpha\beta}$ are the Christoffel symbols. The Christoffel symbols, $\Gamma^\mu_{\alpha\beta}$, can be expressed in terms of the metric tensor $g_{\mu\nu}$ as:

$$\Gamma^\mu_{\alpha\beta} = \frac{1}{2}g^{\mu\sigma}\left(\partial_\alpha g_{\sigma\beta} + \partial_\beta g_{\sigma\alpha} - \partial_\sigma g_{\alpha\beta}\right), \tag{1.5}$$

where $g^{\mu\sigma}$ is the inverse metric tensor, and ∂_α denotes partial differentiation with respect to the coordinate x^α. These symbols encapsulate information about the curvature of spacetime, effectively capturing how gravity influences the path of an object [11].

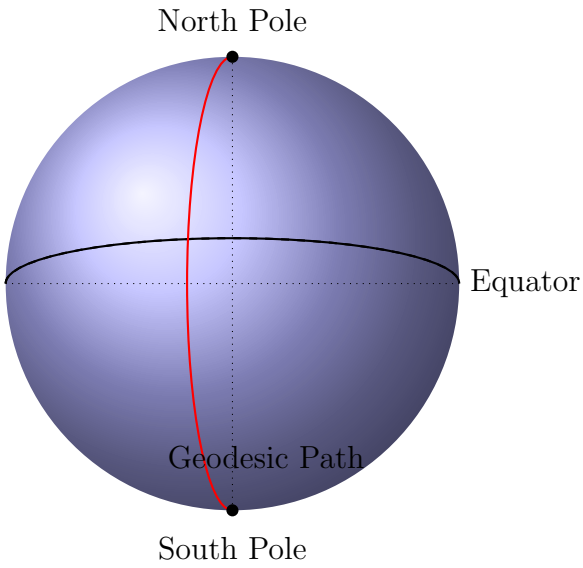

Figure 1.1: Illustration of a geodesic path on a curved sphere. These geodesics are known as great circles.

Null geodesics expressed in Figure 1.2 describe the path taken by massless particles such as photons. A distinctive feature of null geodesics is that the spacetime interval along them is zero. This can be expressed mathematically as:

$$ds^2 = g_{\mu\nu} dx^\mu dx^\nu = 0. \tag{1.6}$$

This zero interval distinguishes null geodesics from timelike or spacelike paths, and it highlights their role in signaling or causal propagation at the speed of light.

In the context of black holes, null geodesics reveal particularly interesting behaviors. Close to a black hole, the gravitational effects become so intense that the paths of null geodesics bend significantly, forming structures like photon spheres. The expansion

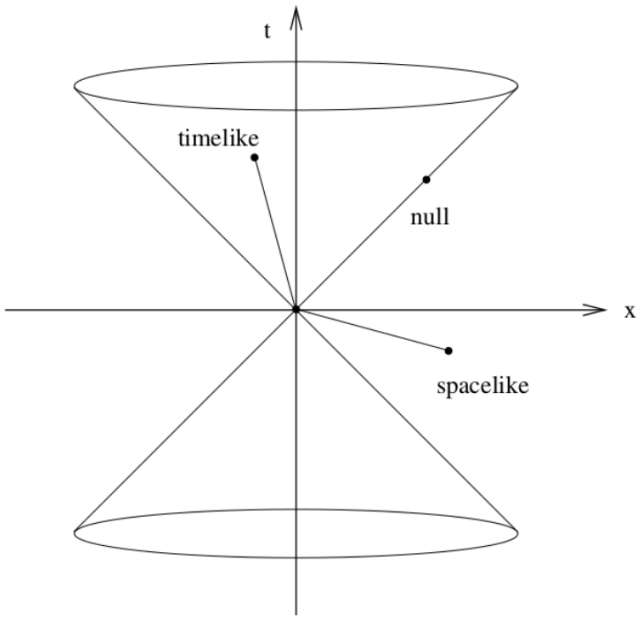

Figure 1.2: In flat Minkowski spacetime, a light-like geodesic is illustrated, as opposed to time-like geodesics and space-like geodesics [32].

scalar, θ, measures the rate at which nearby null geodesics converge or diverge and is defined for an affinely parameterized null geodesic as:

$$\theta = \nabla_a k^a, \tag{1.7}$$

where ∇_a denotes the covariant derivative, and k^a is the tangent vector to the null geodesic [11]. Here, k^a is normalized such that it satisfies the affine parameterization condition, making θ a well-defined measure of expansion along the geodesic. The behavior of the expansion scalar plays a major role in defining trapped surfaces and the event horizons. In flat spacetime, where $\theta > 0$, this means that light rays emitted outwards from a sphere, will diverge. At the event horizon of a stationary black hole, light rays do not converge or diverge and thus satisfy $\theta = 0$. Inside the event horizon, all light rays in any direction converge towards the singularity meet, thereby

indicating $\theta < 0$ [11].

1.3 Trapped Surfaces

A trapped surface is a closed spacelike two-dimensional surface in a four-dimensional spacetime where the expansion of both ingoing and outgoing future-directed null geodesics is everywhere negative. That is, normal light rays, whatever their initial direction, are forced to converge towards each other. Mathematically, for a two-surface (S), we define two null vector fields, (l^a) (outgoing) and (n^a) (ingoing), normalized such that $l \cdot n = -1$ [58]. The concept of trapped surfaces lies at the heart of Penrose singularity theorem: under certain conditions, a trapped surface unavoidably leads to a singularity. This result, depicted in Figure 1.3, below was striking as it showed that singularities are a generic feature of gravitational collapse, not only an artifact of highly symmetric situations, as was believed before [40]. Consequently, trapped surfaces are often used as local indicators of black hole regions. Unlike the event horizon, which is a global concept that requires the knowledge of future spacetime, trapped surfaces can be identified locally, making them invaluable in numerical relativity [54]. The apparent horizon is the boundary for the union of all trapped surfaces in a given spacelike slice of spacetime. The concept is very important in numerical relativity when tracing the evolution of black holes in simulations [5]. Table 1.1 shows the classification of closed surfaces based on their null expansion [50].

1.4 Marginally Outer Trapped Surfaces (MOTS)

Let us consider a four-dimensional time-orientable spacetime (M, g_{ab}) and a two-dimensional spacelike surface S embedded within it. To understand MOTS, we first

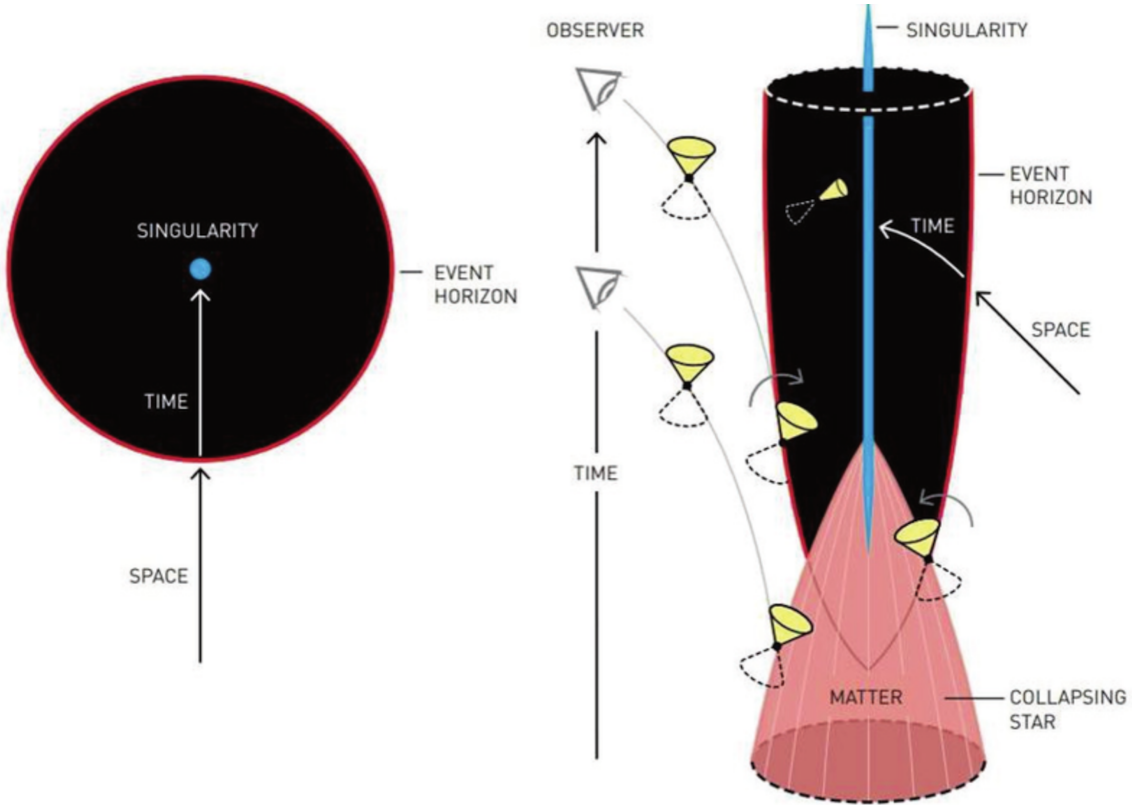

Figure 1.3: This diagram is based on Penrose's paper from 1965 showing the collapse of matter into a black hole. On a trapped surface, all light cones are pointed inwards and the singularity formation is inevitable. Credit: Royal Swedish Academy Of Science [19]

need to establish a clear notion of "inside" and "outside" for S [1]. This distinction allows us to define future-oriented outward-pointing (l^a) and inward-pointing (n^a) null normal vectors to S. The expansions along these null directions are given by:

$$\theta_{(l)} = \tilde{q}^{ab}\nabla_a l_b \quad \text{and} \quad \theta_{(n)} = \tilde{q}^{ab}\nabla_a n_b, \tag{1.8}$$

where $\tilde{q}^{ab}$ is the projection operator onto S, defined as:

$$\tilde{q}^a_b = g^a_b + l^a n_b + n^a l_b. \tag{1.9}$$

Surface Type	$\theta_{(l)}$	$\theta_{(n)}$	**Physical Interpretation**
Untrapped	> 0	< 0	Light rays diverge in one direction, converge in the other
Trapped	< 0	< 0	Light rays converge in both directions
Outer-trapped	< 0	No restriction	Outgoing light rays converge
Marginally outer trapped	$= 0$	No restriction	Outgoing light rays neither converge nor diverge
Bifurcating	$= 0$	$= 0$	Both ingoing and outgoing light rays are stationary

Table 1.1: Classification of Closed Surfaces Based on Null Expansions

These expansions represent the rate of change of the surface area along the respective null directions [6]. In flat spacetime, we would expect $\theta_{(l)} > 0$ and $\theta_{(n)} < 0$, indicating an area increase for outward deformations and a decrease for inward deformations. A surface S is classified as a Marginally Outer Trapped Surface (MOTS) if:

$$\theta_{(l)} = 0. \tag{1.10}$$

This condition signifies that light rays emitted orthogonally from S in the outward direction have zero expansion, neither converging nor diverging to the first order [4]. The classification of surfaces based on the signs of $\theta_{(l)}$ and $\theta_{(n)}$ is invariant under rescaling of the null vectors. For any function F, if we rescale the null vectors as:

$$l^a \to e^F l^a \quad \text{and} \quad n^a \to e^{-F} n^a, \tag{1.11}$$

the expansions transform as $\theta_{(l)} \to e^F \theta_{(l)}$ and $\theta_{(n)} \to e^{-F}\theta_{(n)}$, preserving their signs [29]. The full extrinsic geometry of a two-surface is characterized not only by the expansions $\theta_{(l)}$ and $\theta_{(n)}$, but also by the shears $\sigma^{ab}_{(l)}$ and $\sigma^{ab}_{(n)}$, and the curvature of the normal bundle Ω_{ab}. These quantities are related to the variation of the induced metric $\tilde{q}_{ab}$ under deformations:

$$\delta_l \tilde{q}_{ab} = \frac{1}{2}\theta_{(l)}\tilde{q}_{ab} + \sigma_{(l)ab} \quad \text{and} \quad \delta_n \tilde{q}_{ab} = \frac{1}{2}\theta_{(n)}\tilde{q}_{ab} + \sigma_{(n)ab}. \tag{1.12}$$

The curvature of the normal bundle is given by:

$$\Omega_{ab} = d_a\tilde{\omega}_b - d_b\tilde{\omega}_a, \tag{1.13}$$

where d_a is the induced covariant derivative on S and $\tilde{\omega}_a = -\tilde{q}^b_a n_c \nabla_b l^c$ is the connection on the normal bundle [7]. The stability of MOTS is of particular interest, as it provides information about the evolution of black hole horizons. For a MOTS S, we can study its stability by considering variations of $\theta_{(l)}$. In vacuum spacetimes, these variations are given by:

$$\delta_l \theta_{(l)} = -\sigma^{ab}_{(l)}\sigma^{(l)}_{ab}, \tag{1.14}$$

$$\delta_n \theta_{(l)} = -\frac{1}{2}\tilde{R} - d_a\tilde{\omega}^a + \tilde{\omega}_a\tilde{\omega}^a, \tag{1.15}$$

where $\tilde{R}$ is the Ricci scalar of S [7]. These variations allow us to classify MOTS further. Following Hayward's classification [29], a MOTS is an outer trapping horizon if there exists a scaling of the null vectors such that $\delta_n\theta_{(\ell)} < 0$. This condition ensures that the MOTS can be infinitesimally deformed into an outer trapped surface. The relationship between MOTS and event horizons is a subject of great importance in black hole physics. As Wald emphasizes [58], the evolution of light rays from a MOTS

is intimately connected to the null energy condition:

$$R_{ab}l^a l^b \geq 0, \tag{1.16}$$

and the asymptotic structure of spacetime.

MOTS are guaranteed to either lie within or coincide with the event horizon. The causal character of the time evolved apparent horizon (often a marginally outer trapped tube, MOTT, which consists of a collection of such MOTS forming a tube-like structure) can vary [6] :

- When $R_{ab}l^a l^b = 0$, the MOTT is null and non-expanding.
- When $R_{ab}l^a l^b > 0$, the MOTT is spacelike and expanding.

These conditions provide us with a rich framework for understanding the dynamics of black hole horizons in various physical scenarios.

1.4.1 Types of Marginally Outer Trapped Surfaces

There are various types of MOTS. Bifurcating MOTS occur when a single MOTS splits into two distinct surfaces or, conversely, when two MOTS merge into one. The work of Pook-Kolb et al. [41] on binary black hole mergers beautifully illustrates this phenomenon. A typical merger scenario starts with two stable MOTS representing the individual black holes. As they approach each other, a new pair of MOTS which enclose the original black hole appears – one stable and one unstable. The stable one grows to become the apparent horizon of the merged black hole, while the unstable one shrinks and eventually meets the two original MOTS.

The self-intersecting MOTS, another type of MOTS was first discovered in numerical

simulations of binary black hole mergers [41], and challenged our intuitive understanding of black hole boundaries. These MOTS form when the inner common MOTS hugs the individual black hole MOTS, even after they have merged. This results in a surface that passes through itself, creating a complex, pretzel-like structure as shown in Figure (1.4) below:

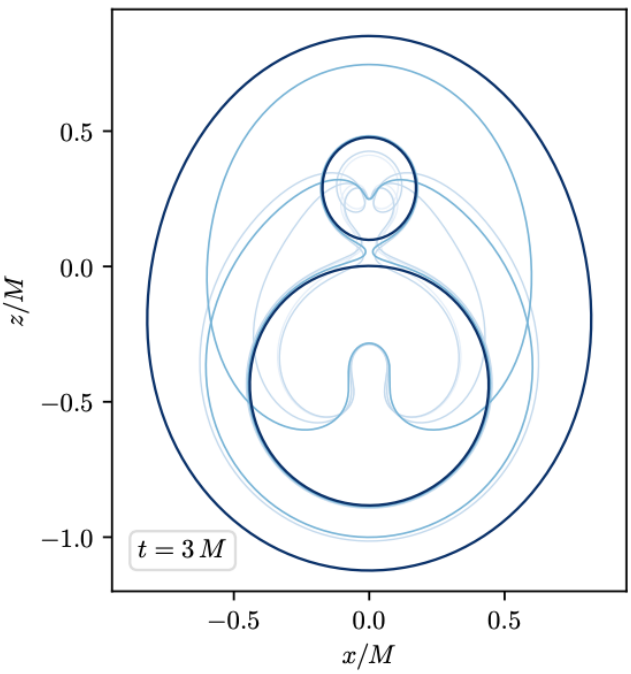

Figure 1.4: Examples of self-intersecting MOTSs exhibiting complex pretzel-like structures. The figure shows a variety of MOTSs, including surfaces with self-intersections. The three dark curves correspond to S_{outer} and $S_{1,2}$, while the lighter curves indicate surfaces with increasing instability. The presence of self-intersections highlights the intricate geometry of these surfaces [42]

.

A Dynamical Horizon is a MOTT. They are spacelike hypersurfaces foliated by MOTS [6]. Tracking the evolution of dynamical horizons provides a powerful tool for understanding the growth and properties of black holes in dynamic spacetimes.

1.5 Stability Analysis

Unlike the intuitive notion of stability in physics, which often relates to how systems respond to perturbations over time, the stability of MOTS is a geometric concept. It fundamentally concerns the behavior of the surface under infinitesimal deformations and its role in delineating trapped and untrapped regions of spacetime. At the heart of MOTS stability analysis lies the stability operator, often denoted as L. This operator, when applied to MOTS, yields information on how the expansion of outgoing null geodesics changes under infinitesimal deformation of the surface. The eigenvalue spectrum of L, particularly its principal (lowest) eigenvalue, determines the stability characteristics of the MOTS. A MOTS is considered stable if its principal eigenvalue is non-negative. This geometric stability implies that the MOTS is "isolated". In a specific sense: any small outward deformation of the surface results in an untrapped surface, while any small inward deformation yields a trapped surface [3]. This property is crucial for understanding the role of MOTS as a boundary between trapped and untrapped regions in spacetime. The vanishing of the principal eigenvalue often signifies a critical point in the evolution of spacetime geometry. Such moments can correspond to the formation of a new black hole or to instances where an existing black hole begins to lose its distinct identity in regions of intense gravitational fields [6]. These transitions between stability and instability are not mere mathematical curiosities, but have profound implications for our understanding of gravitational collapse and black hole dynamics. A geometrically stable MOTS can exist in dynamically evolving spacetimes, including those describing collapsing stars or merging black holes.

In the context of Weyl-distorted Schwarzschild spacetimes, the stability analysis of MOTS becomes particularly intriguing. The introduction of distortions breaks the

spherical symmetry of the Schwarzschild solution; as the distortion parameters vary, we expect to see transitions between stable and unstable configurations, offering insights into how external influences can affect the fundamental nature of black hole horizons. Understanding these stability properties is not just a matter of mathematical interest. It has practical implications for numerical relativity, where the identification and tracking of MOTS play a crucial role in simulating black hole spacetimes. Stable MOTS are typically easier to locate and track numerically, while the presence of unstable MOTS can indicate regions where careful numerical techniques are required [52]. As we delve deeper into the stability analysis of MOTS in Weyl-distorted Schwarzschild spacetimes, we must keep in mind that we are probing the very nature of black hole boundaries. The interplay between spacetime geometry, gravitational fields, and the behavior of null geodesics encapsulated in the MOTS stability problem offers a window into the fundamental structure of gravity in strong-field regimes.

1.6 Research Objectives and Motivation for Study

The primary objective of this research is to investigate the stability properties of Marginally Outer Trapped Surfaces (MOTS) in Weyl-distorted Schwarzschild spacetimes through a rigorous analysis of the associated eigenvalue problem. This study aims to bridge the gap between idealized black hole solutions and more realistic astrophysical scenarios, providing insights into the behavior of black hole horizons under external influences. Our research is motivated by several key factors:

1. Understanding Transitions in Spacetime Geometry: The moments when the principal eigenvalue of the stability operator vanishes are of particular interest. These instances often signify critical transitions in the spacetime geometry, such

as the formation of new black holes or the merging of existing ones. By carefully mapping out these transitions as functions of the distortion parameters, we aim to construct a more complete picture of how black holes evolve and interact in complex gravitational environments [6].

2. Informing Numerical Relativity: Our analytical study of MOTS stability in Weyl-distorted Schwarzschild spacetimes has significant implications for numerical relativity. The insights gained from this work can inform the development of more robust algorithms for horizon tracking in numerical simulations, particularly in situations involving strong gravitational fields or complex matter distributions [52].

3. Bridging Idealized Models and Astrophysical Reality: While the Schwarzschild solution provides a beautiful and analytically tractable model of a black hole, it represents an idealized scenario rarely, if ever, realized in nature. As Thorne and Hartle eloquently argued, astrophysical black holes are invariably subject to external influences that distort their spacetime geometry [55]. By introducing Weyl distortions, we take a significant step towards modeling more realistic black hole environments. This approach allows us to systematically study how various astrophysical factors—such as tidal forces from nearby objects, surrounding matter distributions, or passing gravitational waves—affect the fundamental properties of black holes.

Chapter 2

MATHEMATICAL AND THEORETICAL FOUNDATION

2.1 The Schwarzschild Solution

The general form of the metric for a static, spherically symmetric, asymptotically flat spacetime in vacuum is:

$$ds^2 = -(1 - 2Gm/r)dt^2 + (1 - 2Gm/r)^{-1}dr^2 + r^2(d\theta^2 + \sin^2\theta d\phi^2). \tag{2.1}$$

In this equation, m represents the mass of the central object and G is the gravitational constant [12]. The Schwarzschild metric reveals several fascinating properties of spacetime around a non-rotating, uncharged black hole, with perhaps the most captivating feature being the event horizon [14]. At the heart of the black hole, at $r = 0$, the metric predicts a true singularity [28]. At this point, the curvature of spacetime becomes infinite. These properties are illustrated in Figure (2.1) below. Other key features of the metric include: asymptotic flatness which implies that as

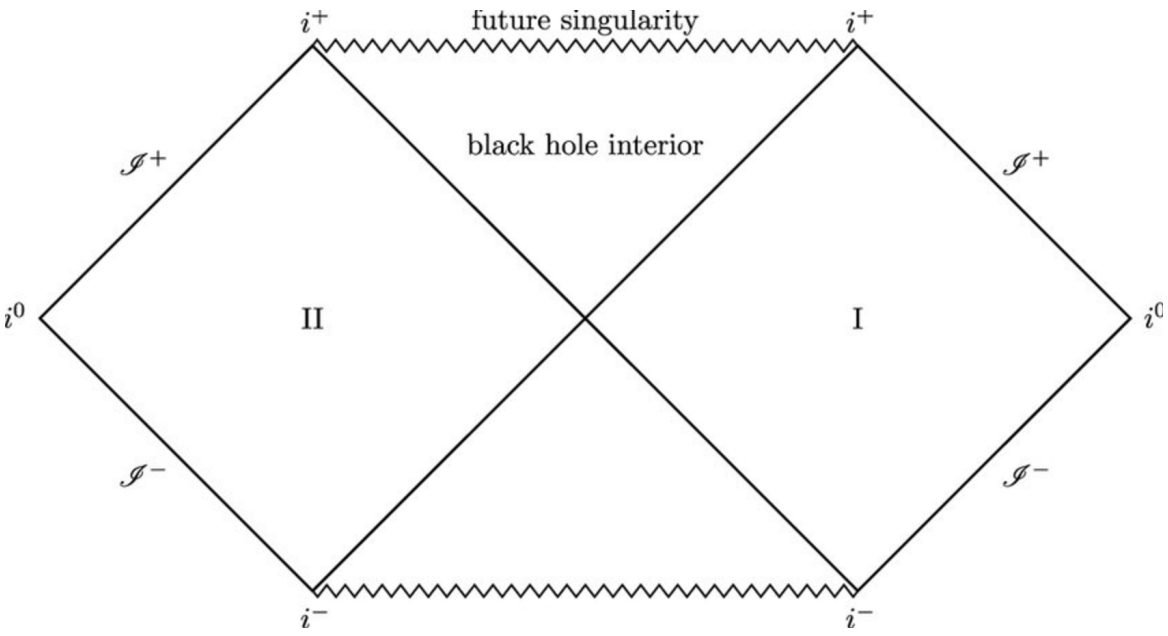

Figure 2.1: Penrose diagram for the maximally extended Schwarzschild spacetime. The diagram shows the causal structure of the eternal black hole solution, including two asymptotically flat regions (I and II). The zigzag lines represent the curvature singularities at $r = 0$. Key features: i^0 (spatial infinity), $i^\pm$ (future/past timelike infinity), and $\mathscr{I}^\pm$ (future/past null infinity) [11]

we move away from the black hole, that is, as r goes to infinity, the metric gradually transitions to flat Minkowski spacetime, illustrating how the black hole's influence diminishes with distance [48]. Time dilation is another indicator that shows that for a distant observer, time appears to slow dramatically for objects approaching the event horizon [44]. Gravitational redshift means that light emitted near the event horizon experiences a significant redshift, appearing redder to distant observers due to the intense gravitational pull [51].

2.1.1 Limitations and Extensions

Although ground-breaking, the Schwarzschild solution certainly has its own set of limitations. For example, it describes a non-rotating and uncharged black hole in a

vacuum [31, 47, 56], which does not represent the universe in all aspects. In a bid to meaningfully address these limitations, several extensions have been developed:

1. Kerr metric: describes rotating black holes.
2. Reissner-Nordström metric: accounts for charged, non-rotating black holes
3. Kerr-Newman metric: encompasses both charged and rotating black holes
4. The Weyl Class of Solutions: a general framework for studying gravitational fields and their distortions in the course of analyzing static axisymmetric spacetimes [13, 37, 26].

These extensions provide a better framework allowing us to model and study diverse astrophysical scenarios.

2.2 The Weyl-Distorted Schwarzschild Solution

Real astrophysical black holes exist in complex environments, and are subject to various external influences that can distort their spacetime geometry [22]. To model these more realistic scenarios, we turn to the framework of Weyl-distorted Schwarzschild spacetimes.

2.2.1 Formulation in Weyl Distorted Schwarzschild

The power of Weyl coordinates becomes apparent when considering distorted versions of the Schwarzschild spacetime. In these coordinates, the metric for a Weyl-distorted

Schwarzschild spacetime takes the form:

$$ds^2 = -e^{2U}F dt^2 + e^{-2U+2V}\left(\frac{dr^2}{F} + r^2 d\theta^2\right) + e^{-2U} r^2 \sin^2\theta d\phi^2, \tag{2.2}$$

where $F(r) = 1 - \frac{2m}{r}$ is the familiar Schwarzschild factor, with m representing the mass of the black hole [59]. The functions $U(r,\theta)$ and $V(r,\theta)$ are the distortion potentials that encode the deviation from the pure Schwarzschild geometry.

2.2.2 Einstein Field Equations and Distortion Potentials

The vacuum Einstein field equations, when applied to this metric, yield a set of partial differential equations for the distortion potentials. Particularly illuminating are the equations derived from $R_{tt} = 0$ and $R_{\phi\phi} = 0$, which lead to a governing equation for $U(r,\theta)$:

$$\frac{\partial}{\partial r}\Big(r^2 F U_r\Big) + \frac{1}{\sin\theta}\frac{\partial}{\partial\theta}\Big(\sin\theta\, U_\theta\Big) = 0, \tag{2.3}$$

highlighting the harmonic nature of the distortion potential U, as this equation closely resembles the Laplace equation in spherical coordinates [21].

The potential $V(r,\theta)$, on the other hand, is determined by a set of first-order equations derived from the remaining Einstein equations components ($R_{rr} = 0$, $R_{r\theta} = 0$, and $R_{\theta\theta} = 0$):

$$V_r = \frac{1}{\Xi}\left[(r-m)A\sin\theta + B\cos\theta\right], \tag{2.4}$$

$$V_\theta = \frac{1}{\Xi}\left[(r-m)B\sin\theta - r^2 F A\cos\theta\right]. \tag{2.5}$$

Here, we have introduced the auxiliary functions:

$$\Xi = (r-m)^2 - m^2\cos^2\theta, \tag{2.6}$$

$$A = \left(r^2 F U_r^2 + 2mU_r - U_\theta^2\right)\sin\theta, \tag{2.7}$$

$$B = \left(2r^2 F U_r + 2mU_\theta\right)\sin\theta. \tag{2.8}$$

The solutions to these equations, represented by the distortion potentials $U(r,\theta)$ and $V(r,\theta)$, provide a complete description of the distorted spacetime geometry [14].

2.2.3 Exact Series Solution for Distortion Potentials

The beauty of the Weyl formalism lies in its amenability to exact solutions. The general solution to equation (2.3) can be written as an infinite series:

$$U(r,\theta) = \sum_{n=1}^{\infty} \alpha_n \left(\frac{m}{R}\right)^n \mathcal{P}_n, \tag{2.9}$$

where α_n are multipole coefficients that characterize the distortion, and R is defined as:

$$R = \left((1-\frac{2m}{r})r^2 + m^2\cos^2\theta\right)^{1/2}. \tag{2.10}$$

The functions $\mathcal{P}_n$ are related to Legendre polynomials through:

$$\mathcal{P}_n = P_n\left(\frac{(r-m)\cos\theta}{R}\right). \tag{2.11}$$

This series solution provides a powerful tool for analyzing distorted Schwarzschild spacetimes, as it allows for the systematic study of various distortion modes [46]. Given the form of U, it is possible to integrate the differential equations for V to

obtain:

$$V(r,\,\theta) = \sum_{i=1}^{\infty} \frac{i\alpha_i^2}{2} \left(\frac{R}{m}\right)^{2i} \left(\mathcal{P}_i^2 - \mathcal{P}_{i-1}^2\right) \tag{2.12}$$
$$- \frac{1}{m} \sum_{i=1}^{\infty} \alpha_i \sum_{j=0}^{i-1} \Big[(-1)^{i+j} \left(r - m\left(1 - \cos\theta\right)\right) + r - m\left(1 + \cos\theta\right)\Big] \left(\frac{R}{m}\right)^{j} \mathcal{P}_j,$$

This expression for V completes our description of the distorted spacetime geometry. [35].

2.2.4 Horizon Geometry and Simplified Forms

Of particular interest is the behavior of these distortion potentials at the horizon, where $r = 2m$. At this location, the expressions for U and V simplify considerably:

$$R(2m, \theta) = m\cos\theta,\ \mathcal{P}_n(2m, \theta) = 1, \tag{2.13}$$

leading to the horizon forms of the distortion potentials:

$$\bar{U}(\theta) := U(2m, \theta) = \sum_{n=1}^{\infty} \alpha_n \cos^n\theta, \tag{2.14}$$

$$\bar{V}(\theta) := V(2m, \theta) = 2\bar{U}(\theta) - 2u_0. \tag{2.15}$$

where we have introduced:

$$u_0 = \sum_{n=1}^{\infty} \alpha_{2n}. \tag{2.16}$$

These simplified forms provides insight into the geometry of the distorted horizon [20].

2.2.5 Physical Interpretation and Implications

The distortion potentials U and V encode a lot of physical information about the distorted spacetime. The multipole coefficients α_n can be related to external sources of distortion [53]. For instance, the α_1 term corresponds to a dipole distortion, which can be interpreted as a linear acceleration of the black hole. The α_2 term represents a quadrupole distortion, which might arise from tidal forces due to nearby massive objects [21]. Higher-order terms in the expansion capture increasingly complex distortion patterns, allowing for a detailed modeling of various astrophysical scenarios. It's worth noting that odd-order terms in the expansion break the equatorial symmetry of the spacetime, while even-order terms preserve it [46]. The horizon forms of the distortion potentials, $\bar{U}(\theta)$ and $\bar{V}(\theta)$, are particularly significant as they directly influence the intrinsic and extrinsic geometry of the black hole horizon. At $r = 2m$, derived from Equation (2.2), the intrinsic metric on the horizon takes the form:

$$ds_H^2 = 4m^2 e^{-2\bar{U}(\theta)} \left(e^{4U(\theta)-4u_0} d\theta^2 + \sin^2\theta d\phi^2 \right). \tag{2.17}$$

revealing how the distortions affect the shape and size of the horizon [20].

2.3 MOTS in Distorted Spacetimes

On a given spatial slice Σ, a MOTS is characterized by the vanishing expansion of outgoing null geodesics [3]:

$$\theta_{(l)} = \tilde{q}^{ab} \nabla_a l_b = 0, \tag{2.18}$$

where $\tilde{q}^{ab}$ is the induced metric on the surface, and ∇_a is the covariant derivative compatible with the spacetime metric. One of the most striking features of MOTS

in distorted spacetimes is their potential non-uniqueness. During black hole mergers, distorted spacetimes can host multiple MOTS simultaneously [6]. This multiplicity introduces a rich geometry to the space of MOTS, with potential bifurcations as the spacetime evolves. The geometry of MOTS in distorted spacetimes deviates significantly from the perfect spheres obeserved in Schwarzschild solutions. These surfaces can exhibit complex shapes that reflect the underlying distortions of the spacetime. For instance, in axisymmetric distorted spacetimes, MOTS might take on oblate or prolate spheroidal forms, depending on the nature of the distortion [30].

The dynamic behavior of MOTS in distorted spacetimes is particularly fascinating. As the spacetime evolves, we can observe the emergence of new MOTS, the disappearance of existing ones, and even mergers between distinct MOTS. This evolution is intimately tied to the changing geometry of the spacetime.

Another crucial aspect to consider is the selection effect associated with MOTS. Although the identification of MOTS depends on the choice of spatial slicing, their physical significance remains unchanged. As emphasized by Booth [6], the behavior of MOTS across different slicing can provide valuable information about the causal structure of the spacetime. The study of MOTS in distorted spacetimes also has important implications for our understanding of black hole thermodynamics. The area of a MOTS, even in distorted spacetimes, is closely related to the entropy of the black hole [4]. However, the presence of multiple MOTS raises intriguing questions about how to properly account for black hole entropy in these more complex scenarios. In the following chapters, we will explore specific techniques for analyzing MOTS in Weyl-distorted Schwarzschild spacetimes, focusing on the stability operator and its eigenvalue spectrum.

Chapter 3

Marginally Outer Trapped Surfaces and Stability

3.1 MOTS and Deformations

Recall that a marginally outer trapped surface (MOTS) S is a closed space-like two surface where the outward null expansion $\theta_{(l)}$ measures how the area of S changes under infinitesimal deformations along the null direction l^a. By definition, we have:

$$\theta_{(l)} = 0. \tag{3.1}$$

This condition implies that, to first order, the area remains constant when S is deformed along l^a. A classic example of such a surface is the event horizon of a Schwarzschild black hole, which is a null hypersurface with constant area [49]. However, a true black hole horizon must do more than maintain a constant area—it must serve as a boundary separating trapped and untrapped regions of spacetime.

Figure 3.1 illustrates the ideal scenario where a MOTS S is a boundary between

trapped and untrapped regions.

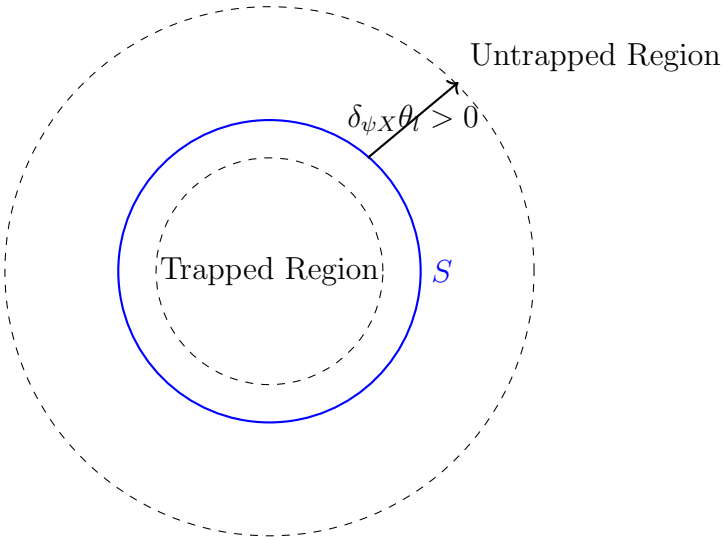

Figure 3.1: Trapped surfaces exist only inside S, while untrapped surfaces exist only outside.

To delve deeper, we consider deformations of S in a general outward direction. As depicted in Figure 3.2, for a general outward-oriented normal vector X^a, our aim is to determine whether trapped surfaces can emerge from such deformations.

For a MOTS S, let l^a and n^a denote its outward and inward null normals, respectively, as shown in Figure 3.3. A general outward normal vector can then be expressed as:

$$X^a = Al^a - Bn^a, \tag{3.2}$$

where $A, B > 0$, and the null vectors l^a and n^a are normalized such that $l^a n_a = -1$. The coefficients are determined as $A = -X^a n_a$ and $B = X^a l_a$. Additionally, we define a rescaled null vector $\ell^a = \mu l^a$, such that the corresponding expansion scales as $\theta_\ell = \mu\theta_l$.

To understand whether S genuinely acts as a boundary between the trapped and untrapped regions, we examine how $\theta_{(l)}$ changes under infinitesimal deformations in

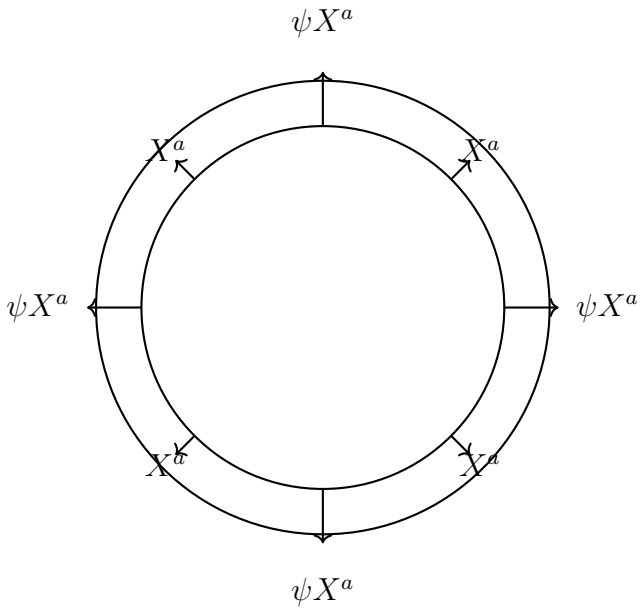

Figure 3.2: Deformation vector field X^a and its scaled version ψX^a, showing the original and deformed surfaces.

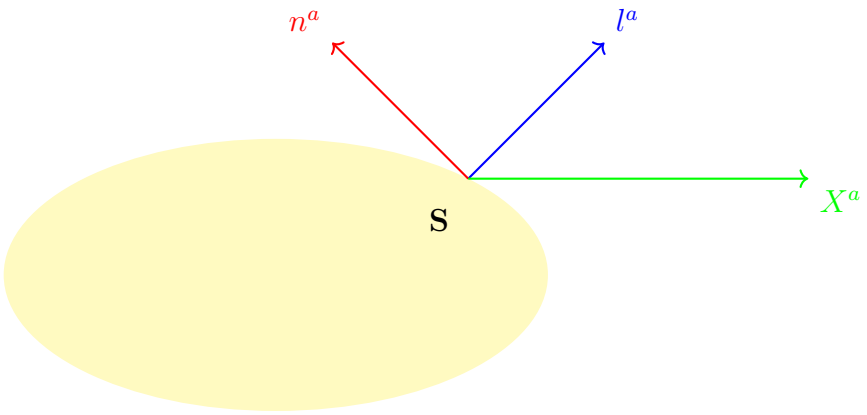

Figure 3.3: The outward and inward null normals l^a and n^a are shown on S

the direction ψX^a. The variation in $\theta_{(l)}$ is given by:

$$\delta_{\psi X}\theta_{(\ell)} = \mu\left(-\mathcal{D}_l^2[B\psi] + \left(BK - A||\sigma_\ell||^2\right)\psi\right), \tag{3.2}$$

where $\mu > 0$ is a scaling factor, $\mathcal{D}_l^2$ is a second-order differential operator, K is the Gaussian curvature of S, and $||\sigma_\ell||^2$ is the squared norm of the shear tensor [9].
The second-order differential operator $\mathcal{D}_l^2$ for a scalar function F is defined as [8]:

$$\mathcal{D}_l^2 F = \left(D_A^l - \omega_A^l\right)\left(D_l^A - \omega_l^A\right)F, \tag{3.3}$$

where w_A^l is the connection term, given by:

$$\omega_A^l = -\tilde{q}_A^a n_c \nabla_a l^c. \tag{3.4}$$

Here, $\tilde{q}_A^a$ project onto the tangent space of S.
From Equation (3.2), several key observations follow:

1. The sign of $\delta_{\psi X}\theta_{(\ell)}$ remains unchanged for any $\mu > 0$. Thus, the specific normalization of ℓ^a does not influence the result.

2. For static MOTS, where $||\sigma_\ell||^2 = 0$, the coefficient A becomes irrelevant and only the component along n^a, determined by B, contributes.

3. The variation $\delta_{\psi X}\theta_{(\ell)}$ is independent of the choice of null vectors l^a and n^a, provided that $\omega_A^l = D_A F$, as is the case here. By choosing l^a and n^a such that $\omega_A^l = 0$, the expression simplifies significantly.

For our purposes, we are mainly concerned with the sign of $\delta_{\psi X}\theta_{(\ell)}$ under various

deformations. This allows us to study the simpler operator [8]:

$$L\psi = -\mathcal{D}^2\psi + K\psi, \tag{3.5}$$

where

$$\mathcal{D}^2 = D^A D_A, \tag{3.6}$$

is the covariant Laplacian on S.

Despite the complexity of the full operator in Equation (3.2), the simpler operator L shares the same number of negative, zero, and positive eigenvalues. As such, analyzing the eigenvalue spectrum of L provides all the information necessary for our investigation. Since L is elliptic and self-adjoint, its eigenvalues are guaranteed to be real, facilitating a straightforward stability analysis.

3.2 The Eigenvalue Problem

The stability of MOTS is intimately connected to the spectral properties of the stability operator L. Since L is a linear elliptic operator, we can formulate an eigenvalue problem:

$$L\psi = \lambda\psi. \tag{3.7}$$

The eigenvalues λ and eigenfunctions ψ of this equation provide crucial information about the stability of the MOTS. For a self-adjoint L, all eigenvalues are real, and we can order them as $\lambda_0 \leq \lambda_1 \leq \lambda_2 \leq \cdots$. The principal eigenvalue λ_0 and its corresponding eigenfunction ψ_0 are of particular importance. A fundamental result in the theory of elliptic operators states that ψ_0 can be chosen to be strictly positive on S [2]. The sign of λ_0 determines the stability of the MOTS: If $\lambda_0 > 0$, the MOTS

is strictly stable. If $\lambda_0 = 0$, the MOTS is marginally stable. If $\lambda_0 < 0$, the MOTS is unstable. The physical interpretation of these eigenvalues is profound. As shown by Andersson, Mars, and Simon [2], the sign of λ_0 determines whether it is possible to deform the MOTS outward to produce a trapped or untrapped surface. Specifically: if $\lambda_0 \geq 0$, no deformation can produce a trapped surface outside the MOTS and S bounds a trapped region. If $\lambda_0 < 0$, there exists a deformation that produces a trapped surface outside the MOTS and S is not a boundary. This result establishes a clear connection between the mathematical properties of the stability operator and the physical concept of trapping. Booth and Fairhurst [9] further extended this analysis, showing that the concept of stability is closely related to the behavior of dynamical horizons and the existence of barriers in black hole spacetimes.

Analytical approaches to solving the eigenvalue problem are generally limited to highly symmetric situations, such as spherical spacetimes. In more general cases, numerical methods are required. These can range from finite difference schemes to spectral methods, depending on the geometry of the problem and the desired accuracy. To gain intuition about the stability operator and its eigenvalues, it's helpful to draw an analogy with concepts from multivariable calculus, particularly the analysis of critical points.

3.2.1 Analogy Between Critical Points in Multivariable Calculus and Stability of MOTS

Consider a smooth scalar function $z = f(x, y)$ defined on a two-dimensional surface. A critical point of this function occurs when the gradient of f vanishes, that is, when

$$\frac{\partial f}{\partial x} = 0 \quad \text{and} \quad \frac{\partial f}{\partial y} = 0. \tag{3.7}$$

This condition mirrors the concept of a marginally outer trapped surface (MOTS), which can be thought of as a critical surface in spacetime geometry [1]. To understand the nature of critical points, we examine the Hessian matrix, which consists of the second partial derivatives of $f(x, y)$:

$$H = \begin{bmatrix} f_{xx} & f_{xy} \\ f_{xy} & f_{yy} \end{bmatrix}, \tag{3.8}$$

where f_{xx}, f_{yy}, and f_{xy} represent the second-order derivatives of f. The **determinant** of the Hessian, denoted D, is given by

$$D = f_{xx}f_{yy} - (f_{xy})^2. \tag{3.9}$$

This determinant plays a crucial role in determining the nature of the critical point:

- If $D > 0$ and $f_{xx} > 0$, the critical point is a **local minimum**.
- If $D > 0$ and $f_{xx} < 0$, the critical point is a **local maximum**.
- If $D < 0$, the critical point is a **saddle point** [39].

The nature of these critical points can also be analyzed using the eigenvalues of the Hessian matrix, λ_1 and λ_2. Consider the eigenvalue equation for the Hessian matrix:

$$H\mathbf{v} = \lambda\mathbf{v},$$

where $\mathbf{v}$ is an eigenvector and λ is the corresponding eigenvalue. Rewriting this, we have:

$$(H - \lambda I)\mathbf{v} = 0.$$

For a non-trivial solution ($\mathbf{v} \neq 0$), the determinant of $(H - \lambda I)$ must vanish:

$$\det(H - \lambda I) = 0.$$

In the case of a 2×2 Hessian matrix, this condition becomes:

$$\det \begin{bmatrix} f_{xx} - \lambda & f_{xy} \\ f_{xy} & f_{yy} - \lambda \end{bmatrix} = 0.$$

Expanding this determinant gives the quadratic equation:

$$(f_{xx} - \lambda)(f_{yy} - \lambda) - f_{xy}^2 = 0.$$

Rewriting this in standard form, we have:

$$\lambda^2 - \text{tr}(H)\lambda + D = 0,$$

where $\text{tr}(H) = f_{xx} + f_{yy}$ is the trace of the Hessian matrix, and $D = f_{xx}f_{yy} - f_{xy}^2$ is its determinant.

The roots of this quadratic equation, λ_1 and λ_2, are the eigenvalues of the Hessian. These eigenvalues determine the nature of the critical point:

- If $D > 0$, the eigenvalues λ_1 and λ_2 have the same sign:
  - If $\text{tr}(H) > 0$, both eigenvalues are positive, indicating a local minimum.
  - If $\text{tr}(H) < 0$, both eigenvalues are negative, indicating a local maximum.
- If $D < 0$, the eigenvalues have opposite signs, corresponding to a saddle point.

The stability of a MOTS is analogous to the behavior of a critical point in multivariable calculus, except it occurs in an infinite-dimensional space of functions. Just as the Hessian matrix provides insights into the local curvature near a critical point, the stability operator L determines the stability of the MOTS by influencing its eigenvalue spectrum. The critical eigenvalue λ_0 plays a key role in determining whether the MOTS is stable [2]. Figure 3.4 illustrates the different types of critical points. A minimum is stable in the sense that a ball sitting at a minimum will stay there. But, for a maximum or saddle point, it could roll downhill and disappear.

Just as the Hessian describes local behavior near a critical point in a two-dimensional surface, the stability operator governs the behavior of the MOTS in the context of spacetime geometry.

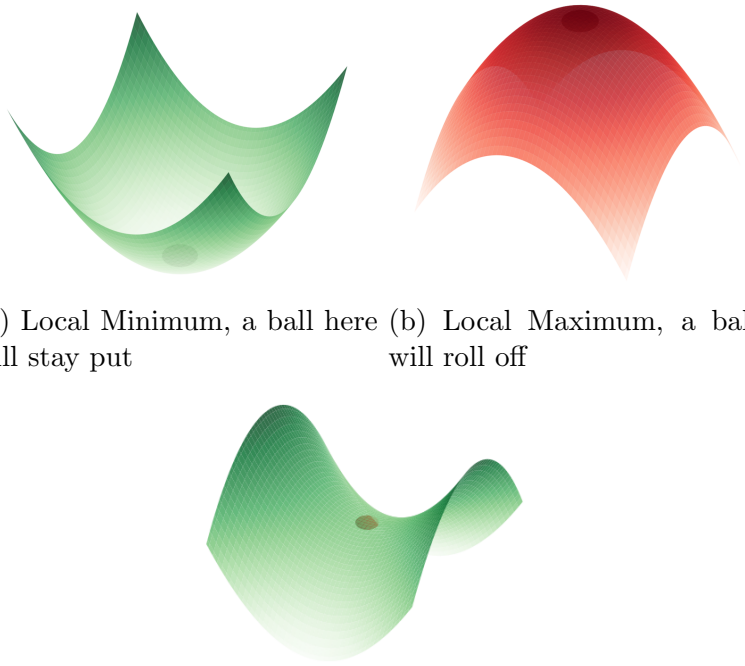

(a) Local Minimum, a ball here will stay put

(b) Local Maximum, a ball will roll off

(c) Marginal Stability

Figure 3.4: Illustration of critical points: a local minimum (stable), a local maximum (unstable), and a saddle point (marginal stability). Each point represents a stability type analogous to MOTS stability.

3.2.2 Implications for Trapped Regions

The stability of marginally outer trapped surfaces (MOTS) significantly impacts the structure of trapped regions in spacetime, particularly in dynamic scenarios like black hole mergers. The evolution of MOTS in these situations is intimately connected to their stability properties.

- Stable MOTS evolve into smooth, continuous world tubes, acting as consistent boundaries of trapped regions. These stable surfaces maintain their integrity throughout the evolution, providing a well-defined structure to the trapped region [43].

- In contrast, unstable MOTS can lead to discontinuous jumps in the apparent horizon, causing sudden changes in the geometry of the trapped region. This illustrates the role stability plays in shaping the behavior of horizons in dynamic spacetimes.

Furthermore, under certain conditions, the stability of MOTS offers valuable insights into the structure of trapped regions. Specifically, in asymptotically flat spacetimes with appropriate energy conditions, the outermost MOTS is necessarily stable. However, a strictly stable MOTS does not have to be the outermost one; it is possible for a strictly stable MOTS to exist within the trapped region, surrounded by another MOTS that serves as the outer boundary [43]. This distinction underscores the geometric complexity of trapped regions and the critical role of stability in understanding their evolution.

Figure 3.5 illustrates the concept of a dynamical horizon and its relation to MOTS stability. In the next chapter, we turn to the numerical methods used to solve the eigenvalue problem in distorted spacetime.

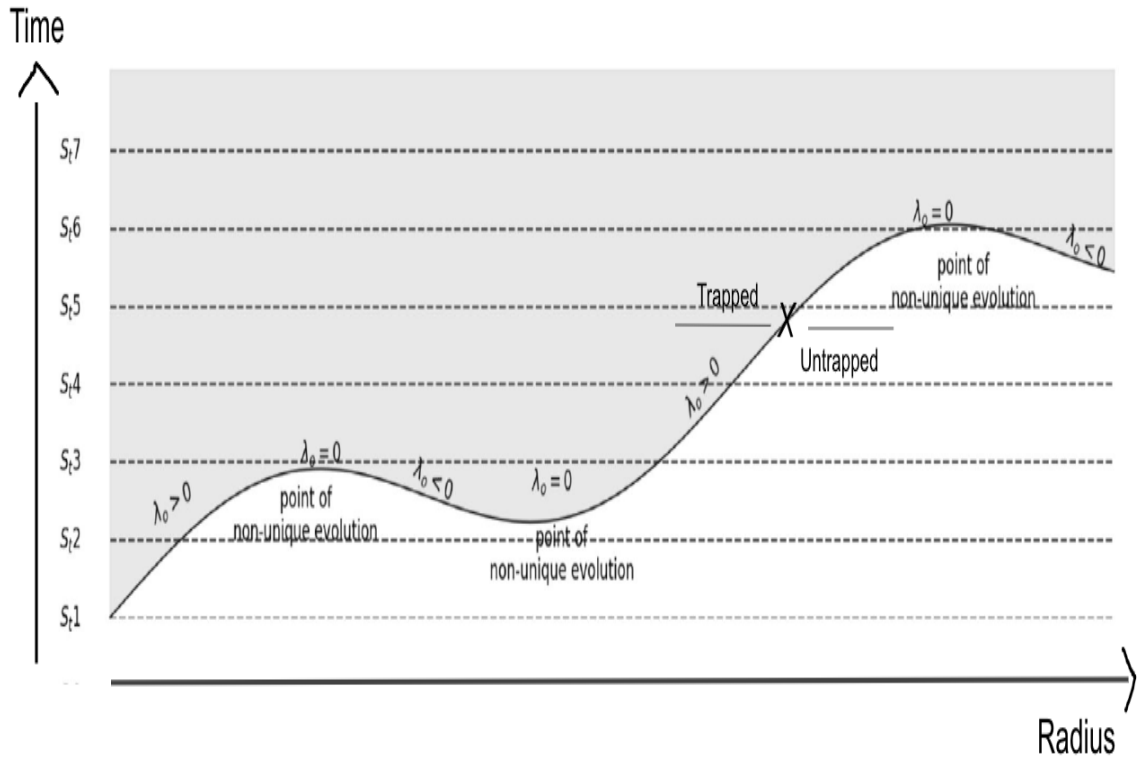

Figure 3.5: Schematic illustration of a dynamical horizon foliated by marginally trapped surfaces S_t [8]. Each point is a sphere. Trapped surfaces are contained in the shaded area. The stability of each S_t influences the evolution of the horizon H.

Chapter 4

Numerical Methods for Eigenvalue Analysis

Recall from equation (2.17), the intrinsic metric on the horizon of the Weyl-distorted Schwarzschild solution is:

$$ds_H^2 = 4m^2 e^{-2\bar{U}(\theta)} \left(e^{4U(\theta)-4u_0} d\theta^2 + \sin^2\theta d\phi^2 \right), \tag{4.1}$$

where $U = U(\theta)$ is the Weyl potential, and u_0 is a constant. The distortion is parameterized by α, with $U = \alpha \cos^2\theta$ for quadrupole distortions.

The stability operator L for MOTS in this spacetime can be derived from the variation of the expansion of outgoing null geodesics. After a series of calculations involving the metric components and their derivatives, for the specific case of quadrupole distortions where $U = \alpha \cos^2\theta$ [8], we calculate the components of equation (3.5) to

obtain:

$$L\psi = \left(-\frac{d^2}{d\theta^2} - \cot\theta\frac{d}{d\theta} + 1\right)\psi \\ + \alpha\left(-4\cos\theta\sin\theta\frac{d}{d\theta} - 10\cos^2\theta + 2\right)\psi + \alpha^2\left(-8\cos^2\theta\sin^2\theta\right)\psi, \tag{4.2}$$

for the axisymmetric ψ. Each component of this expression corresponds to specific terms in Equation (3.5): The first term corresponds to the Laplacian operator on the 2D surface S in spherical coordinates. The other term arises from the linear contributions of the distortion potential. It captures higher-order effects of the distortion. This form of the operator reveals several important features:

1. The undistorted Schwarzschild case is recovered when $\alpha = 0$, reducing to the standard Schwarzschild solution.

2. The distortion introduces coupling between different angular modes, evident in the $\cos^2\theta$ and $\cos\theta\sin\theta$ terms.

3. The operator is self-adjoint, ensuring a real eigenvalue spectrum.

4. The α^2 term suggests non-linear effects for large distortions, potentially leading to rich stability behavior.

Before proceeding with the analysis, it is important to acknowledge the contributions that made this work possible. The comprehensive spectral method analysis and the results derived from it were conducted by my supervisor, Prof. Ivan Booth, while I focused on the finite difference method and obtained the corresponding results. I am deeply grateful for his invaluable guidance and support throughout this research.

4.1 The spectral method

The spectral method approximates the axisymmetric solutions by expanding them in terms of a set of basis functions:

$$\psi(\theta) = \sum_{n=0}^{N} a_n \psi_n(\theta), \tag{4.3}$$

For our axisymmetric MOTS in the Weyl-distorted Schwarzschild spacetime, we employ Chebyshev polynomials $\cos(n\theta)$ as our basis functions, leveraging their orthogonality properties on the interval $[0, \pi]$ [10]. To implement the spectral method for our specific stability operator, we construct a matrix representation of L in the Chebyshev polynomial basis and solve the resulting matrix eigenvalue problem. The matrix elements of L in the Chebyshev basis can be computed using the inner product defined for functions in this basis:

$$\langle \psi_m(\theta), \psi_n(\theta) \rangle = \int_0^{\pi} \psi_m(\theta)\psi_n(\theta)\, d\theta. \tag{4.4}$$

For Chebyshev polynomials, this inner product takes the form:

$$\int_0^{\pi} \cos(m\theta)\cos(n\theta)\, d\theta = \begin{cases} \frac{\pi}{2}\delta_{mn}, & m, n \neq 0, \\ \pi, & m = 0 \text{ and } n = 0, \end{cases}$$

where δ_{mn} is the Kronecker delta, equal to 1 when $m = n$ and 0 otherwise [10]. Taking into account the normalization factor, we can express the matrix elements of L as:

$$L_{mn} = \begin{cases} \frac{1}{\pi}\int_0^{\pi} L[1]\, d\theta, & m = n = 0, \\ \frac{2}{\pi}\int_0^{\pi} \cos(m\theta) L[\cos(n\theta)]\, d\theta, & m, n \neq 0. \end{cases}$$

This integration is more complex than in the simplified case, but can still be performed efficiently using computer algebra [45].

The spectral method offers several advantages for our stability analysis: for smooth solutions (i.e., infinitely differentiable), the spectral method converges exponentially. This means that as the number of basis functions (or grid points) increases, the error decreases exponentially, resulting in very rapid convergence for smooth problems [23]. The method provides high-order accuracy across the entire domain, not just at discrete points.

The finite difference method, on the other hand, usually exhibits algebraic or polynomial convergence. The error decreases at a polynomial rate, which is proportional to the grid spacing. For example, a second-order finite difference method would reduce the error quadratically as the grid is refined, but this is slower than the exponential rate of the spectral method. Thus, the spectral method can provide higher accuracy with fewer grid points for smooth problems, while the finite difference method requires more points to achieve comparable accuracy [34].

4.2 Finite Difference Method

The finite difference method provides a more straightforward approach to discretizing our stability operator, which can be particularly useful given its complex form. To apply the finite difference method to our stability operator, we discretize the θ-domain into N points: $\theta_i = i\Delta\theta$, where $\Delta\theta = \pi/(N+1)$ and $i = 0, 1, \ldots, N+1$. We use the

following finite difference approximations:

$$\left.\frac{d^2\psi}{d\theta^2}\right|_{\theta_i} \approx \frac{\psi_{i+1} - 2\psi_i + \psi_{i-1}}{(\Delta\theta)^2}, \tag{4.5}$$

$$\left.\frac{d\psi}{d\theta}\right|_{\theta_i} \approx \frac{\psi_{i+1} - \psi_{i-1}}{2\Delta\theta}. \tag{4.6}$$

Applying these approximations to our stability operator yields a discrete eigenvalue problem:

$$\begin{aligned} &-8\alpha^2 \cos^2\theta_i \sin^2\theta_i \psi_i + \Bigg(\Big(-4\frac{\psi_{i+1} - \psi_{i-1}}{2\Delta\theta}\cos\theta_i \sin\theta_i - \\ &10\cos^2\theta_i\psi_i + 2\psi_i\Big)\alpha - \frac{\psi_{i+1} - \psi_{i-1}}{2\Delta\theta}\cot\theta_i - \frac{\psi_{i+1} - 2\psi_i + \psi_{i-1}}{(\Delta\theta)^2} + \psi_i\Bigg) = \lambda\psi_i. \end{aligned} \tag{4.7}$$

This can be written as a matrix eigenvalue problem $A\psi = \lambda\psi$, where A is a tridiagonal matrix with additional terms from the α-dependent parts of the operator.

The finite difference method is generally stable for well-posed problems, but care must be taken when dealing with singular terms, because near the poles ($\theta = 0$ and $\theta = \pi$), these terms can lead to large errors or instabilities. The accuracy of the finite difference method is typically of order $O(\Delta\theta^2)$ for second-order central differences. This means that to improve accuracy by a factor of 10, we need to increase the number of grid points by a factor of $\sqrt{10} \approx 3.16$.

The finite difference method, which is the approach I used for this study on the Weyl-distorted stability operator, faces several challenges: the accuracy of the finite difference approximation may degrade near the boundaries of the domain, and capturing the behavior of highly distorted solutions (large α) may require a finer grid [34]. To address these issues, we can employ techniques such as using a staggered grid that avoids the poles.

The spectral method and the finite difference method give consistent results when used to study the stability operator, provided that sufficient resolution is used in both methods and boundary conditions are handled properly [34].

4.3 Numerical Challenges and Solutions

The numerical analysis of MOTS stability presents several challenges that require careful consideration and innovative solutions.

4.3.1 Handling Coordinate Singularities

The axisymmetric nature of the problem introduces coordinate singularities at the poles ($\theta = 0$ and $\theta = \pi$). To address this, the Chebyshev polynomial basis we initially employed inherently satisfies the correct boundary behavior. This choice of basis ensures that the solutions have regularity at the poles, eliminating the need for explicit boundary conditions and avoiding issues related to the coordinate singularity [10].

4.3.2 Convergence Analysis

To ensure the reliability of our results, we performed a convergence analysis. We compute the eigenvalues for increasing resolution (higher N or finer grid spacing) and monitor the change in eigenvalues [34].

These solutions provide confidence in the accuracy and reliability of our numerical framework, ensuring that the results obtained for distorted spacetimes are trustworthy and physically meaningful.

In the next chapter, we'll study the results obtained from applying these numerical methods to investigate the stability spectrum of MOTS in the Weyl-distorted Schwarzschild spacetimes, exploring how different distortion parameters affect the eigenvalue distribution and the implications for black hole stability and dynamics.

Chapter 5

Results and Analysis

5.1 Eigenvalue Spectrum for Varying Distortion Parameters

Recall that stable Marginally Outer Trapped Surfaces (MOTS) provide a localized and geometrically defined boundary between trapped and untrapped regions of spacetime, making them invaluable for understanding black hole stability and dynamics. This chapter presents the results of the eigenvalue spectrum analysis for the MOTS stability operator. The spectral and finite difference numerical methods were employed to compute these spectra, each offering unique insights into the stability properties of MOTS in Weyl-distorted Schwarzschild spacetimes.

5.1.1 Results from the Spectral Method

The spectral method revealed a systematic transition of the eigenvalues as the distortion parameter increased, reflecting the destabilizing effect of external distortions

on the MOTS geometry. It is important to note that the operator that was analyzed via the spectral method differs slightly from its extended counterpart which was analyzed using the finite difference method (FDM), due to the inclusion of an additional exponential term, $e^{-2\bar{U}+4u_0}$. This term was incorporated in the spectral analysis done by Prof. Booth [8]. While this term scales the eigenvalues spectrum, it does not alter their qualitative nature—whether they are positive, negative, or zero. Figure 5.1 illustrates the eigenvalue distribution as a function of the distortion parameter α. This

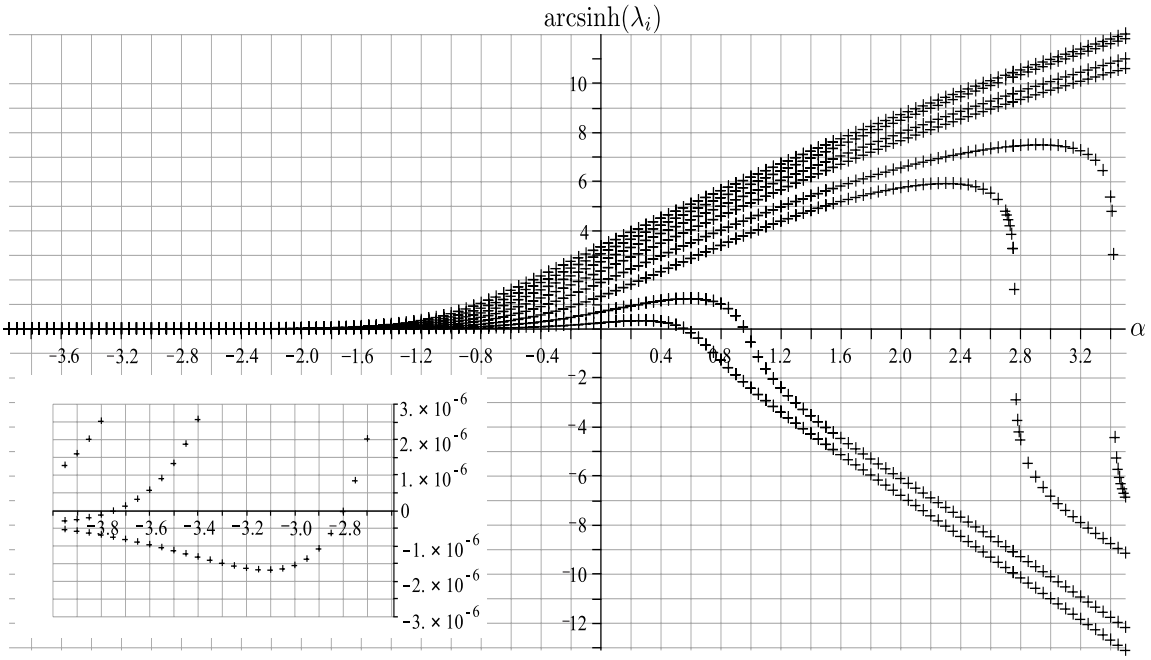

Figure 5.1: Eigenvalue spectrum for varying distortion parameter α. Eigenvalues are labelled from lowest to highest as $\lambda_0, \lambda_1, ..., \lambda_7$.

plot, adapted from the work of [8], showcases the behavior of the first eight eigenvalues $\lambda_i\,(i = 0, \ldots, 7)$ as functions of α.

The principal eigenvalue, λ_0, which determines the geometric stability of the MOTS, is of particular interest. As α approaches certain critical values, the spectral method identifies the vanishing of λ_0, marking transitions to marginal stability. These transitions are pivotal, as they signal geometric configurations where the MOTS ceases

to act as a stable boundary, potentially foreshadowing phenomena such as black hole mergers or the emergence of new trapped surfaces. To complement these results, we present, in the next section, the corresponding eigenvalue spectrum analysis using the finite difference method.

5.1.2 Results from the Finite Difference Method

The finite difference method offered a complementary approach to solving the eigenvalue problem. Recall that, for this study, the stability operator was discretized over a uniform grid in θ, with careful treatment of boundary conditions to avoid artifacts near the poles. The finite difference results illustrated in figure 5.2 corroborated the spectral method's findings, demonstrating consistent eigenvalue trends across the range of distortion parameter. However, the finite difference method required a higher

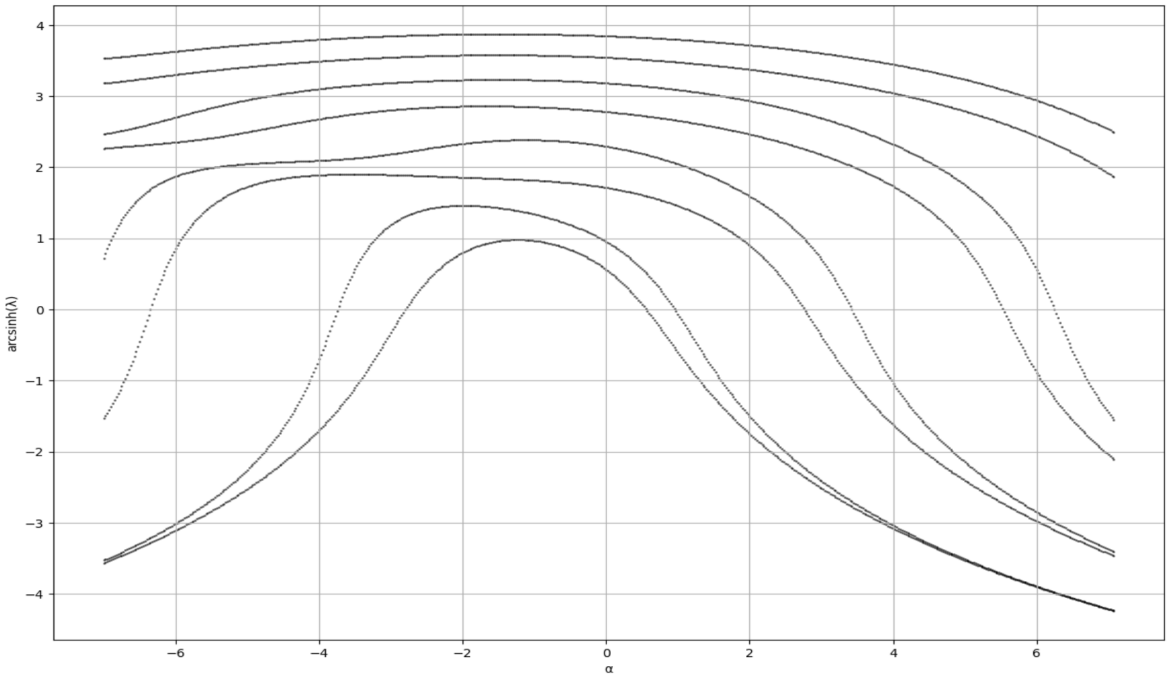

Figure 5.2: Eigenvalue spectrum for varying distortion parameter α (FDM). Again, eigenvalues are labelled from lowest to highest as $\lambda_0, \lambda_1, ..., \lambda_7$.

resolution to achieve comparable accuracy, particularly for higher-order eigenvalues. The principal eigenvalue (λ_0) exhibited with the FDM trends consistent with the spectral analysis, further validating the reliability of the numerical framework.

5.2 Principal Eigenvalue Analysis

The behavior of the principal eigenvalue reveals several key features. For $\alpha = 0$, we recover the known result for the Schwarzschild horizon, where the principal eigenvalue is positive [11]. For large α, the principal eigenvalue appears to decrease monotonically, ensuring a transition to instability for sufficiently large distortions. The intriguing extremely and important aspect of the principal eigenvalue stability analysis is the identification of critical transition points at $\alpha = -2.798086$ and 0.557798. Between these points, the horizon is a stable MOTS, and so is a boundary between the trapped and untrapped region. Outside of this range, it is no longer a boundary. The emergence of a negative principal eigenvalue in extreme gravitational distortion conditions suggests the possible formation of new MOTS. From these findings illustrated in Figure 5.3, we may state that "moderately" distorted black holes, characterized by the distortion parameter, maintain stable horizons.

5.3 Comparative Analysis of Numerical Methods

The points at which the stability operator vanishes hold significant physical and mathematical implications. For each eigenvalue, these points represent critical values of the distortion parameter α, where the stability characteristics of the MOTS undergoes a fundamental change. These stability transitions hold profound implications for the causal structure of the distorted spacetime, potentially signaling the formation or

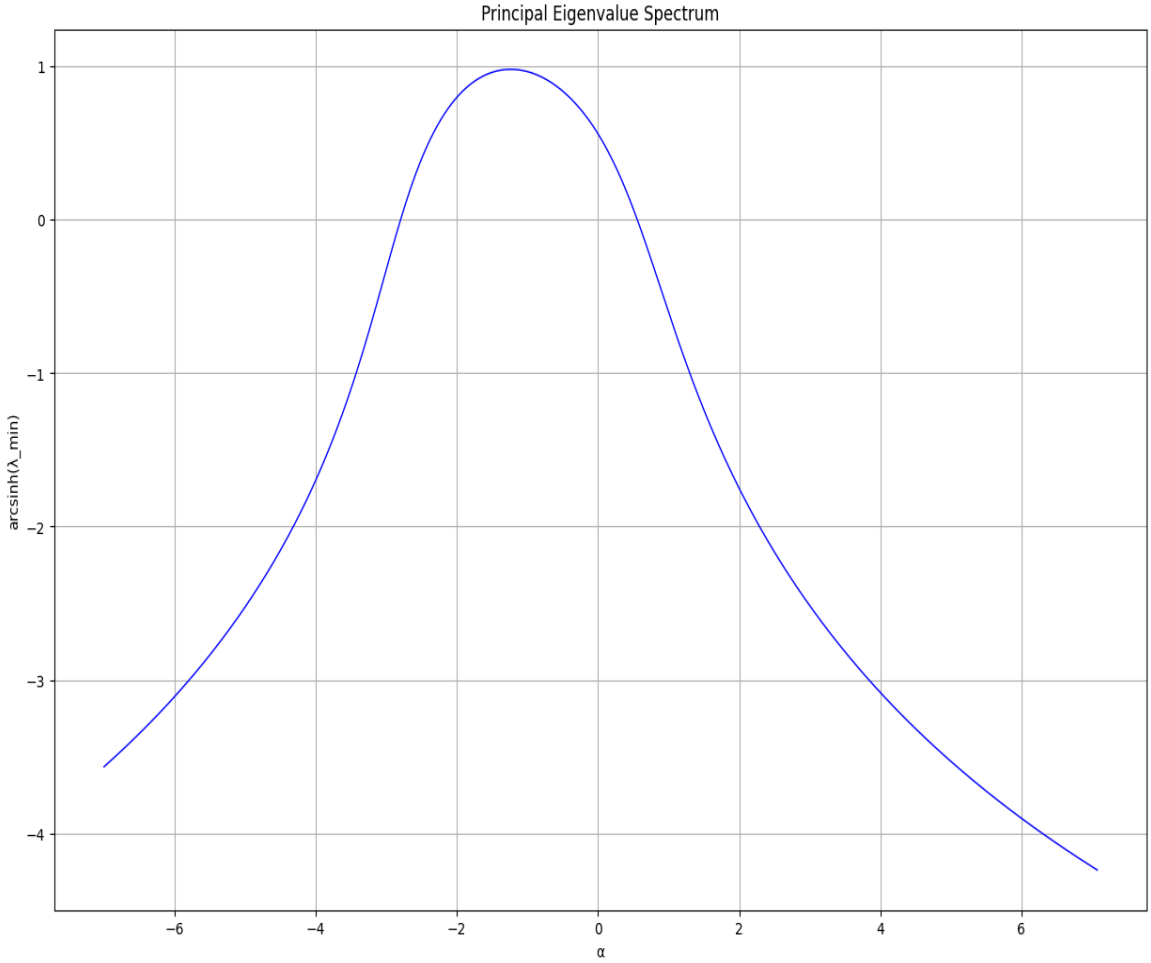

Figure 5.3: Principal eigenvalue as a function of distortion parameter $\alpha(FDM)$.

"dissolution" of black hole horizons. Table 5.1 lists these points derived from both numerical methods. The fact that these points were consistent across both methods evident in figure 5.1 and 5.2 reinforces their significance.

Both methods were implemented using identical boundary conditions and parameter ranges. Figure 5.4 shows a comparison of the first real eigenvalue computed using both methods. Overall, we observe strong consistency between these two methods, particularly for the lower eigenvalues and moderate values of α. For larger values of α, the FDM results show more deviation from the spectral method. To achieve comparable accuracy with the finite difference method for large α, we would need

Methods	λ_0	λ_1	λ_2	λ_3
Spectral	0.557798	0.956652	2.762154	3.422026
FDM	0.577999	0.950023	2.780006	3.442222
Spectral	-2.798086	-3.695085	-6.349868	7.096823
FDM	-2.802086	-3.691115	-6.333561	7.196823

Table 5.1: Comparison of results for values of α for which L vanishes between both methods. This would mean at these points of α, the eigenvalue of $L = 0$

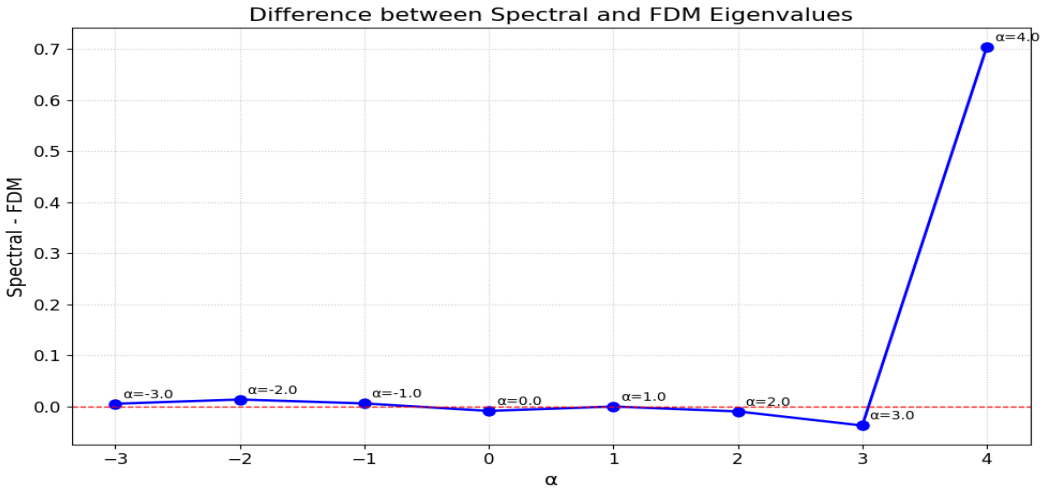

Figure 5.4: Difference plot of the principal eigenvalues computed using spectral and finite difference methods

to significantly increase our grid resolution and unfortunately, such high resolution calculations are computationally intensive and exceed our current resources.

5.3.1 Discussion of Numerical Accuracy and Efficiency

The observed discrepancies between the spectral and FDM results can be attributed to the inherent strengths and limitations of each method:

- Spectral method Pros: Achieves exponential convergence for smooth solutions, providing high accuracy with relatively few basis functions [10].

  Cons: Can suffer from Gibbs phenomena near discontinuities or in regions of rapid variation [24].

- Finite difference method Pros: Conceptually simple and easy to implement, works well for a wide range of problems [34].

  Cons: Typically achieves only polynomial convergence, requiring finer grids for high accuracy [57].

The spectral method exhibits faster convergence, achieving machine precision with fewer than 100 basis functions for moderate α. The FDM, while slower to converge, shows steady improvement with increasing grid resolution.

Chapter 6

Conclusions and Future Work

6.1 Summary of Key Findings

This thesis has explored the stability of Marginally Outer Trapped Surfaces (MOTS) in Weyl-distorted Schwarzschild spacetimes through a comprehensive eigenvalue analysis. Our investigation has mapped the eigenvalue spectrum across a wide range of distortions. The most striking findings are:

1. **Eigenvalue Spectrum Behavior:** We observed a distinct dependence of the eigenvalue spectrum on the distortion parameter α. As α increased, a trend of decreasing eigenvalues emerged. These findings indicate that stronger distortions have a more pronounced impact on the stability properties of MOTS.

2. **The identification of critical values of α where the principal eigenvalue λ_0 vanishes:** These points mark transitions in the stability regime of the MOTS. This result is particularly relevant in the context of binary black hole mergers, where extreme distortions can occur. Our analysis suggests that during such

events, there is a range over which the MOTS remains stable. Outside of this range it is unstable, potentially leading to the formation of new horizons. The behavior of the eigenvalue spectrum in highly distorted regimes aligns with the concept of "black hole dissolution" proposed in recent literature [8]. Our work provides a mathematical foundation for this phenomenon, suggesting that under extreme distortions, the very nature of black hole horizons may fundamentally change.

3. **Physical Implications:** Our analysis suggests that the Weyl-distorted Schwarzschild spacetimes can indeed support stable MOTS for a range of distortion parameters. There exists a critical distortion beyond which the MOTS no longer bound a trapped region. The transition from stable to unstable MOTS indicates a fundamental change in the black hole structure.

6.2 Limitations of the Current Study

While our investigation has yielded valuable insights, it is important to acknowledge the limitations of our approach and the assumptions underlying our analysis. Firstly, our study focused on axisymmetric distortions of the Schwarzschild spacetime. While this provides a tractable model for investigating MOTS stability, it does not capture the full complexity of astrophysical black holes, which may be subject to non-axisymmetric distortions and may possess intrinsic angular momentum. Secondly, our numerical methods, while robust for a wide range of distortion parameters, showed limitations in capturing the behavior of extremely distorted spacetimes. The finite difference method, in particular, required prohibitively high resolutions to achieve accuracy comparable to the spectral method in these regimes. Lastly, while our study

provides insights into the stability characteristics of MOTS, it does not directly address the formation mechanism of these surfaces in dynamical spacetimes.

6.3 Suggestions for Future Research

The findings and limitations of our current study point to several promising avenues for future research:

1. Extension to Kerr Spacetimes: A natural extension of our work would be to analyze MOTS stability in distorted Kerr spacetimes. This would allow us to investigate the interplay between black hole spin and external distortions, providing a more complete picture of astrophysical black hole stability. The stability operator in this case would take the form: text $\tilde{L}_{\text{Kerr}} = \tilde{L}_{\text{Schw}} + \tilde{L}_{\text{spin}} + \tilde{L}_{\text{dist-spin}}$ where $\tilde{L}_{\text{spin}}$ represents the contribution from black hole spin and $\tilde{L}_{\text{dist-spin}}$ captures the coupling between spin and distortion [61].

2. Non-axisymmetric Distortions: Expanding our analysis to include non-axisymmetric distortions would provide a more realistic model of astrophysical environments. This would require modifying our stability operator to include ϕ-dependent terms: $\tilde{L}_{\text{non-axi}} = \tilde{L}_{\text{axi}} + f(\theta, \phi, \alpha)$ where $f(\theta, \phi, \alpha)$ represents the non-axisymmetric contribution.

3. Higher-dimensional Generalizations: Extending our analysis to higher-dimensional spacetimes could provide insights into the stability of black objects in string theory and other higher-dimensional gravity theories. The stability operator in D dimensions would take the form: $\tilde{L}_D = -\Delta_{D-2} + K_{D-2} + Q_D$ where Δ_{D-2} is the Laplacian on the $(D-2)$-dimensional MOTS, K_{D-2} is the extrinsic curvature, and Q_D represents additional geometric terms specific to higher dimensions [18].

4. Numerical Relativity Simulations: Incorporating our MOTS stability analysis into full numerical relativity simulations of binary black hole mergers could provide new insights into horizon dynamics during these extreme events. This would involve tracking the evolution of the stability operator and its eigenvalues throughout the merger process: $\tilde{L}(t)\psi_i(t) = \lambda_i(t)\psi_i(t)$ where $\psi_i(t)$ and $\lambda_i(t)$ represent the time-evolving eigenfunctions and eigenvalues [25]. The most detailed of such analysis was done in [43].

Building upon the methods developed in this work, we are currently studying spacetime near distorted Schwarzschild surfaces to identify and analyze nearby MOTS. A key aspect of this investigation is the study of critical points where the principal eigenvalue of the stability operator vanishes. At these points, we anticipate that the MOTS may separate from the $r = 2m$ surface (the Schwarzschild horizon in the undistorted case). This ongoing research [8] aims to uncover the interplay between neighboring MOTS and the outermost stable surface, further enriching our understanding of the structure of trapped regions. Results from this study will be detailed in our upcoming work [8].

In conclusion, our study of MOTS stability in Weyl-distorted Schwarzschild spacetimes has opened up numerous exciting possibilities for future research. By addressing the limitations of the current work and pursuing these suggested avenues, we can continue to deepen our understanding of black hole physics and the fundamental nature of distorted spacetime.

Bibliography

[1] Lars Andersson, Marc Mars, and Walter Simon. Local existence of dynamical and trapping horizons. *Physical Review Letters*, 95(11):111102, 2005.

[2] Lars Andersson, Marc Mars, and Walter Simon. Stability of marginally outer trapped surfaces and existence of marginally outer trapped tubes. *Advances in Theoretical and Mathematical Physics*, 12(4):853–888, 2007.

[3] Lars Andersson and Jan Metzger. The area of horizons and the trapped region. *Communications in Mathematical Physics*, 290(3):941–972, 2009.

[4] Abhay Ashtekar and Badri Krishnan. Isolated and dynamical horizons and their applications. *Living Reviews in Relativity*, 7(1):10, 2004.

[5] Thomas W. Baumgarte and Stuart L. Shapiro. *Numerical Relativity: Solving Einstein's Equations on the Computer*. Cambridge University Press, 2010.

[6] Ivan Booth. Black-hole boundaries. *Canadian Journal of Physics*, 83(11):1073–1099, 2005.

[7] Ivan Booth. Spacetime near isolated and dynamical horizons. *Physical Review*, 87:024008, 2016.

[8] Ivan Booth, G. Cox, and Chiamaka Mary Okpala. Blackhole dissolution. Unpublished manuscript.

[9] Ivan Booth and Stephen Fairhurst. Isolated, slowly evolving, and dynamical trapping horizons: Geometry and mechanics from surface deformations. *Physical Review D*, 75(8), 2007.

[10] John P Boyd. *Chebyshev and Fourier spectral methods*. Courier Corporation, 2001.

[11] Steven Carlip. *General Relativity: A Concise Introduction*. Oxford University Press, 2019.

[12] Sean M. Carroll. *Spacetime and Geometry: An Introduction to General Relativity*. Addison-Wesley, 2004.

[13] B. Carter. Global structure of the kerr family of gravitational fields. *Physical Review*, 174(5):1559–1571, 1968.

[14] S. Chandrasekhar. *The Mathematical Theory of Black Holes*. Oxford University Press, 1998.

[15] Frank W. Dyson, Arthur S. Eddington, and Charles Davidson. A determination of the deflection of light by the sun's gravitational field, from observations made at the total eclipse of may 29, 1919. *Philosophical Transactions of the Royal Society A*, 220:291–333, 1920.

[16] Albert Einstein. Die feldgleichungen der gravitation. *Sitzungsberichte der Preussischen Akademie der Wissenschaften zu Berlin*, page 844–847, 1915.

[17] Albert Einstein. Kosmologische betrachtungen zur allgemeinen relativitätstheorie. *Sitzungsberichte der Königlich Preussischen Akademie der Wissenschaften*, page 142–152, 1917.

[18] Roberto Emparan and Harvey S. Reall. Black holes in higher dimensions. *Living Reviews in Relativity*, 11:6, 2008.

[19] Viktor Fedorov, Istvan Hargittai, and V.M. Tyutyunnik. Nobel prize winner in physics roger penrose. *Polymers for Advanced Technologies*, 7:168–171, 10 2022.

[20] V. P. Frolov and I. D. Novikov. *Black hole physics: basic concepts and new developments*. Springer Science Business Media, 1998.

[21] Robert Geroch. Multipole moments. ii. curved space. *Journal of Mathematical Physics*, 11(8):2580–2588, 1970.

[22] Robert Geroch and James B. Hartle. Distorted black holes. *Journal of Mathematical Physics*, 23(4):680–692, 1982.

[23] David Gottlieb and Steven A. Orszag. The analysis of spectral methods for hyperbolic initial-boundary value problems. *SIAM Journal on Numerical Analysis*, 14(6):915–930, 1977.

[24] David Gottlieb and Chi-Wang Shu. The gibbs phenomenon and its resolution. *SIAM Review*, 39(4):644–668, 1997.

[25] Ian Hawke, Frank Löffler, and Denis Pollney. Evolution of black holes in numerical relativity. *Classical and Quantum Gravity*, 22(17):S279–S288, 2005.

[26] S. W. Hawking and R. Penrose. The singularities of gravitational collapse and cosmology. *Proceedings of the Royal Society A: Mathematical, Physical and Engineering Sciences*, 314(1519):529–548, 1970.

[27] Stephen W. Hawking. *A Brief History of Time*. Bantam Books, 1988.

[28] Stephen W. Hawking and George F. R. Ellis. *The Large Scale Structure of Space-Time*. Cambridge University Press, 1973.

[29] Sean A Hayward. General laws of black-hole dynamics. *Physical Review D*, 49(12):6467, 1994.

[30] José L. Jaramillo. Black hole dynamics and trapping horizons in numerical relativity. *Living Reviews in Relativity*, 16(1):1–40, 2013.

[31] Roy P. Kerr. Gravitational field of a spinning mass as an example of algebraically special metrics. *Physical Review Letters*, 11(5):237–238, 1963.

[32] M. Kersting. Visualizing four dimensions in special and general relativity. In B. Sriraman, editor, *Handbook of the Mathematics of the Arts and Sciences*, chapter 120. Springer, Cham, 2021.

[33] Urbain J. Le Verrier. Théorie du mouvement de mercure. *Annales de l'Observatoire de Paris*, 5:1–195, 1859.

[34] Randall J. LeVeque. *Finite Difference Methods for Ordinary and Partial Differential Equations: Steady-State and Time-Dependent Problems*. SIAM, Philadelphia, PA, 2007.

[35] V. S. Manko and I. D. Novikov. Generalizations of the kerr and kerr-newman metrics possessing an arbitrary set of mass-multipole moments. *Classical and Quantum Gravity*, 9(11):2477–2487, 1992.

[36] Charles W. Misner, Kip S. Thorne, and John Archibald Wheeler. *Gravitation*. W. H. Freeman and Company, 1973.

[37] E. T. Newman, E. Couch, K. Chinnapared, A. Exton, A. Prakash, and R. Torrence. Metric of a rotating, charged mass. *Journal of Mathematical Physics*, 6(6):918–919, 1965.

[38] Isaac Newton. *Philosophiæ Naturalis Principia Mathematica*. Royal Society, 1687.

[39] MIT OpenCourseWare. Critical points, 2010. Accessed: 2024-11-30.

[40] Roger Penrose. Gravitational collapse and space-time singularities. *Physical Review Letters*, 14(3):57–59, 1965.

[41] Daniel Pook-Kolb, Ofek Birnholtz, Badri Krishnan, and Erik Schnetter. Existence and stability of marginally trapped surfaces in black-hole spacetimes. *Physical Review D*, 99(6):064005, 2019.

[42] Daniel Pook-Kolb, Robie A. Hennigar, and Ivan Booth. What happens to apparent horizons in a binary black hole merger? *Physical review letters*, 127 18:181101, 2021.

[43] Daniel Pook-Kolb, Robie A. Hennigar, and Ivan Booth. What happens to apparent horizons in a binary black hole merger? *Physical Review Letters*, 127(18), 2021.

[44] R. V. Pound and G. A. Rebka. Gravitational red-shift in nuclear resonance. *Physical Review Letters*, 3(9):439–441, 1959.

[45] William H. Press, Saul A. Teukolsky, William T. Vetterling, and Brian P. Flannery. *Numerical Recipes 3rd Edition: The Art of Scientific Computing*. Cambridge University Press, 2007.

[46] H. Quevedo. General static axisymmetric solution of einstein's vacuum field equations in prolate spheroidal coordinates. *Physical Review D*, 39(10):2904, 1991.

[47] H. Reissner. Über die eigengravitation des elektrischen feldes nach der einsteinschen theorie. *Annalen der Physik*, 355(9):106–120, 1916.

[48] B. F. Schutz. *A First Course in General Relativity*. Cambridge University Press, 2009.

[49] Karl Schwarzschild. Über das gravitationsfeld eines massenpunktes nach der einsteinschen theorie. *Sitzungsberichte der Königlich Preussischen Akademie der Wissenschaften*, page 189–196, 1916.

[50] Senovilla and Jose L. Jaramillo. Trapped surfaces. *International Journal of Modern Physics D*, 20(11):2139–2168, October 2011.

[51] I. I. Shapiro. Fourth test of general relativity. *Physical Review Letters*, 13(26):789–791, 1964.

[52] Jonathan Thornburg. Event and apparent horizon finders for 3+ 1 numerical relativity. *Living Reviews in Relativity*, 10(1):3, 2007.

[53] Kip S. Thorne. Multipole expansions of gravitational radiation. *Reviews of Modern Physics*, 52(2):299–339, 1980.

[54] Kip S. Thorne. *Black Holes and Time Warps: Einstein's Outrageous Legacy*. W. W. Norton Company, 1994.

[55] Kip S. Thorne and James B. Hartle. Laws of motion and precession for black holes and other bodies. *Physical Review D*, 31(8):1815, 1985.

[56] R. C. Tolman. Static solutions of einstein's field equations for spheres of fluid. *Physical Review*, 55(4):364–373, 1939.

[57] Lloyd N. Trefethen. *Finite Difference and Spectral Methods for Ordinary and Partial Differential Equations*. Cornell University, 1996.

[58] Robert M. Wald. *General Relativity*. University of Chicago Press, Chicago, 1984.

[59] H. Weyl. Zur gravitationstheorie. *Annalen der Physik*, 359(18):117–145, 1917.

[60] Clifford M. Will. *Theory and Experiment in Gravitational Physics*. Cambridge University Press, 2018.

[61] Shuanglong Zhou et al. Kerr black hole shadows in melvin magnetic field with stable photon orbits. *arXiv preprint arXiv:2104.12304*, 2021. Available at: https://arxiv.org/abs/2104.12304.

6.4 Appendix A Snippet of code: Finite difference method MOTS finding (Principal Eigenvalue)

Here is the Maple code:

```
n := 1000;
theta_vals := Vector(n, i -> evalf(Pi*i/(n + 1)));
diff_matrix_2nd := Matrix(n, n, (i, j) -> piecewise(i = j, -2,
abs(i - j) = 1, 1, 0))*(n + 1)^2/Pi^2;
diff_matrix_2nd := diff_matrix_2nd + Matrix(n, n, (i, j) ->
piecewise(i = 1 and j = 1 or i = n and j = n, -1, i = 1 and j = 2 or
i = n and j = n - 1, 1, 0));
diff_matrix_1st := Matrix(n, n, 0);
for i to n do
```

```
    if 1 < i then diff_matrix_1st[i, i - 1] := -1; end if;
    if i < n then
        diff_matrix_1st[i, i + 1] := 1;
    end if;
end do;
diff_matrix_1st := diff_matrix_1st*(n + 1)/(2*Pi);
for i in {1, n} do
    for j to n do diff_matrix_1st[i, j] := 0; end do;
end do;
create_operator_matrix := proc(alpha_val) local c0,
c1, L, Id, c0_matrix, c1_matrix;
c0 := Vector(n, i -> -8*alpha_val^2*cos(theta_vals[i])^2*
sin(theta_vals[i])^2 -
10*alpha_val*cos(theta_vals[i])^2
+ 2*alpha_val + 1);
c1 := Vector(n, i -> -4*alpha_val*cos(theta_vals[i])*
sin(theta_vals[i]) - cot(theta_vals[i]));
c0_matrix := DiagonalMatrix(c0);
c1_matrix := DiagonalMatrix(c1);
Id := IdentityMatrix(n);
L := c0_matrix + (c1_matrix . diff_matrix_1st) - diff_matrix_2nd;
return L; end proc;
alpha_vals := [seq(-7 + 0.1*i, i = 0 .. 110)];
eigenvalues_list := [];
for a in alpha_vals do
    L := create_operator_matrix(a);
```

```
    ev := Eigenvalues(L);
    eigenvalues_list := [op(eigenvalues_list), [a, min(evalf(ev))]];
end do;
eigenvalues_matrix := Matrix(eigenvalues_list);
```